



OPEN

Serological fingerprints link antiviral activity of therapeutic antibodies to affinity and concentration

Sebastian Fiedler^{1✉}, Sean R. A. Devenish¹, Alexey S. Morgunov^{1,2}, Alison Ilsley¹, Francesco Ricci¹, Marc Emmenegger³, Vasilis Kosmoliaptis^{4,5,6}, Elitza S. Theel⁷, John R. Mills^{8,9}, Anton M. Sholukh¹⁰, Adriano Aguzzi³, Akiko Iwasaki^{11,12,13,14}, Andrew K. Lynn¹ & Tuomas P. J. Knowles^{1,2,15✉}

The effectiveness of therapeutic monoclonal antibodies (mAbs) against variants of the SARS-CoV-2 virus is highly variable. As target recognition of mAbs relies on tight binding affinity, we assessed the affinities of five therapeutic mAbs to the receptor binding domain (RBD) of wild type (A), Delta (B.1.617.2), and Omicron BA.1 SARS-CoV-2 (B.1.1.529.1) spike using microfluidic diffusional sizing (MDS). Four therapeutic mAbs showed strongly reduced affinity to Omicron BA.1 RBD, whereas one (sotrovimab) was less impacted. These affinity reductions correlate with reduced antiviral activities suggesting that affinity could serve as a rapid indicator for activity before time-consuming virus neutralization assays are performed. We also compared the same mAbs to serological fingerprints (affinity and concentration) obtained by MDS of antibodies in sera of 65 convalescent individuals. The affinities of the therapeutic mAbs to wild type and Delta RBD were similar to the serum antibody response, indicating high antiviral activities. For Omicron BA.1 RBD, only sotrovimab retained affinities within the range of the serum antibody response, in agreement with high antiviral activity. These results suggest that serological fingerprints provide a route to evaluating affinity and antiviral activity of mAb drugs and could guide the development of new therapeutics.

The SARS-CoV-2 B.1.1.529.1 variant (Omicron BA.1) was first reported in Botswana and in South Africa in November 2021 and was classified as a variant of concern by the world health organization (WHO) on 26th November 2021^{1,2}. By mid-December 2021, the Omicron BA.1 variant was detected in more than 30 countries and by late January 2022 was the dominant lineage worldwide.

The Omicron BA.1 variant is characterized by a large number of mutations present in the spike and nucleocapsid proteins. Most critical for viral fitness and immune evasion are likely 34 mutations within the Omicron BA.1 spike protein with 10 mutations within the N-terminal domain, 15 in the receptor binding domain (RBD), 3 related to the furin cleavage site and 6 in the S2 region (Tables S1 and S2). Of these mutations, 13 had been

¹Fluidic Analytics, Unit A, The Paddocks Business Centre, Cherry Hinton Road, Cambridge CB1 8DH, UK. ²Yusuf Hamied Department of Chemistry, Centre for Misfolding Diseases, University of Cambridge, Lensfield Road, Cambridge CB2 1EW, UK. ³Institute of Neuropathology, University of Zurich, 8091 Zurich, Switzerland. ⁴Department of Surgery, University of Cambridge, Addenbrookes Hospital, Cambridge CB2 0QQ, UK. ⁵NIHR Blood and Transplant Research Unit in Organ Donation and Transplantation, University of Cambridge, Hills Road, Cambridge CB2 0QQ, UK. ⁶NIHR Cambridge Biomedical Research Centre, Hills Road, Cambridge CB2 0QQ, UK. ⁷Division of Clinical Microbiology, Department of Laboratory Medicine and Pathology, Mayo Clinic, Rochester, MN, USA. ⁸Department of Laboratory Medicine and Pathology, Mayo Clinic, Rochester, MN, USA. ⁹Center for MS and Autoimmune Neurology, Mayo Clinic, Rochester, MN, USA. ¹⁰Vaccine and Infectious Disease Division, Fred Hutchinson Cancer Research Center, Seattle, WA, USA. ¹¹Department of Immunobiology, Yale School of Medicine, New Haven, CT 06519, USA. ¹²Department of Epidemiology of Microbial Diseases, Yale School of Public Health, New Haven, CT 06510, USA. ¹³Department of Molecular, Cellular and Developmental Biology, Yale University, New Haven, CT 06511, USA. ¹⁴Howard Hughes Medical Institute, Chevy Chase, MD 20815, USA. ¹⁵Cavendish Laboratory, Department of Physics, University of Cambridge, JJ Thomson Ave, Cambridge CB3 0HE, UK. ✉email: sebastian.fiedler@fluidic.com; tpjk2@cam.ac.uk

observed in previous variants of SARS-CoV-2 but never in a single lineage, as summarized in Tables S1 and S2. Despite this large number of mutations, Omicron BA.1 still utilizes angiotensin converting enzyme (ACE2) as host receptor and binds with similar affinity as the original Wuhan strain (referred to as wild type throughout the paper)^{3,4}.

Omicron BA.1 mutations reduce the virus neutralization efficacy of some approved or clinical-stage antibody drugs. Casirivimab/imdevimab (Regeneron) and bamlanivimab/etesevimab (Lilly) lose their ability to neutralize, while cilgavimab/tixagevimab (AstraZeneca) and sotrovimab (GSK) retain some degree of efficacy^{3,5–9}.

Virus neutralization of Omicron BA.1 is also strongly reduced in sera from convalescent individuals infected with prior lineages and in the sera of double-vaccinated individuals who had been vaccinated with BNT162b2, mRNA-1273, Ad26.COV2.S, ADZ1222, Sputnik V, or BBIBP-CorV^{3,6,9–11}. Triple vaccinated individuals who have received BNT162b2 or mRNA-1273 also show reduced neutralization efficacy against Omicron BA.1 relative to wild type and Delta, although the retained efficacies are considerably higher than for convalescent or double-vaccinated individuals^{3,6,8,9}. Also, individuals who had been infected with either Delta or an earlier variant of SARS-CoV-2 and subsequently been vaccinated retained considerable titers of neutralizing antibodies (NAbs)^{3,8,9}.

The ability of the Omicron BA.1 variant to evade humoral immune responses, whether induced by infection or vaccination, is expected to cause more reinfections and breakthrough infections. Despite reports of a higher proportion of Omicron BA.1 infections leading to milder disease outcomes^{12–17}, very high case numbers resulting from a more transmissible Omicron BA.1 variant would still pose a significant public health risk.

Here, we used microfluidic diffusional sizing (MDS)^{18–22} to measure the in-solution binding affinities to the spike RBD of the wild type, Delta and Omicron BA.1 variants of five therapeutic monoclonal antibodies (casirivimab, imdevimab, sotrovimab, tixagevimab, and cilgavimab) administered to reduce SARS-CoV-2 viral load and alleviate COVID-19 symptoms. All five antibodies bind wild type and Delta SARS-CoV-2 spike with high affinities and are potent virus neutralizing agents²³. For four of these five drugs, the affinity for the Omicron BA.1 spike RBD was more than two orders of magnitude lower than the affinity for the wild type spike RBD; by contrast, sotrovimab retained significantly higher affinity for the Omicron BA.1 spike RBD. The MDS-based antibody affinities determined were consistent with published virus-neutralization IC₅₀ values (Pearson correlation coefficient $R = 0.8$, p -value = 1.4×10^{-7}) and provide a quantitative explanation for the relative efficacies of all five antibodies against Omicron BA.1. We also considered the affinities of these five mAbs to spike RBDs of the wild type, Delta, and Omicron BA.1 variants in the context of antibody fingerprints, consisting of affinity and concentration data, obtained from the sera of COVID-19 convalescents by microfluidic antibody affinity profiling (MAAP)^{18–21}. MAAP showed that wild type and Delta spike RBD affinities of all five therapeutic antibodies were within the affinity range typical of polyclonal anti-wild type spike RBD antibodies generated by the humoral immune response. Against Omicron BA.1 spike RBD, only sotrovimab stayed within this affinity range, while the other four mAbs had affinities several orders of magnitude lower than antibodies found in convalescent individuals. We also utilized MAAP to fingerprint the antibody response against wild type, Delta and Omicron BA.1 spike RBDs in the working reagent for anti-SARS-CoV-2 immunoglobulin²⁴, a pooled plasma standard from individuals who recovered from COVID-19 in 2020. We observed considerable cross-reactivity to Omicron BA.1 spike RBD and roughly half the concentration of binding antibodies as compared with wild type and Delta.

Results and discussion

The binding affinities of cilgavimab, tixagevimab, sotrovimab, casirivimab, and imdevimab to Omicron BA.1 spike RBD, Delta spike RBD, and wild type spike RBD were determined by MDS (Fig. 1). To do so, equilibrium binding curves were acquired by titrating each antibody against constant concentrations of each spike RBD. The formation of RBD–antibody complexes was monitored based on an increase of the hydrodynamic radius (R_h) of the RBD species in solution.

At the lowest antibody concentrations, in the absence of binding, wild type, Delta, and Omicron BA.1 spike RBDs displayed R_h values of 3.40 nm (SD = 0.27 nm), as observed previously^{18,20,21}.

Notably, the K_D values measured here using microfluidic diffusional sizing are in agreement with published values obtained by surface plasmon resonance (SPR)^{3,4,23}.

Therapeutic antibody binding to Omicron BA.1 RBD was previously reported in a study using bio-layer interferometry (BLI)⁵, which detected no binding for imdevimab, consistent with the MDS results found here. By contrast, the BLI results in the same study reported a low nanomolar affinity to Omicron BA.1 for cilgavimab and sub-nanomolar affinities for tixagevimab, sotrovimab, and casirivimab⁵—results that differ strongly from the affinity values determined by MDS in our present study that show reduced affinity of all four of these mAbs for Omicron BA.1. Given the density of mutations in Omicron BA.1 it seems likely that the affinity determined by BLI is artefactual, a possibility supported by the observation of lost neutralization efficacy for most of these antibodies when challenged with the Omicron BA.1 variant^{3,5–9}.

As shown in Fig. 2, the five antibodies tested have different epitopes on the RBD depending on their modes of action. Cilgavimab and tixagevimab are used as a combination drug, bind to non-overlapping epitopes, and inhibit ACE2 binding^{28–30}. Cilgavimab binds both the up and down conformation of RBD while tixagevimab exclusively binds to the up conformation. For cilgavimab, the substitutions N440K and G446S are likely to affect binding and neutralization. Tixagevimab binds to the left shoulder of RBD with Omicron BA.1 RBD mutations S477N, T478K, and E484A likely to interfere with binding and neutralization. Sotrovimab binds outside the receptor binding motif to a site that involves the N343-linked glycan^{30,31}. This epitope might be sensitive to G339D and N440K substitutions in the Omicron BA.1 spike. Casirivimab and imdevimab prevent viral spike proteins from binding to ACE2²³. The epitope of casirivimab overlaps with the ACE2 binding site, whereas imdevimab binds on the side of the RBD and sterically blocks ACE2 from accessing the spike protein. The binding epitopes of both antibodies contain Omicron BA.1 mutations: for casirivimab the mutations K417N,

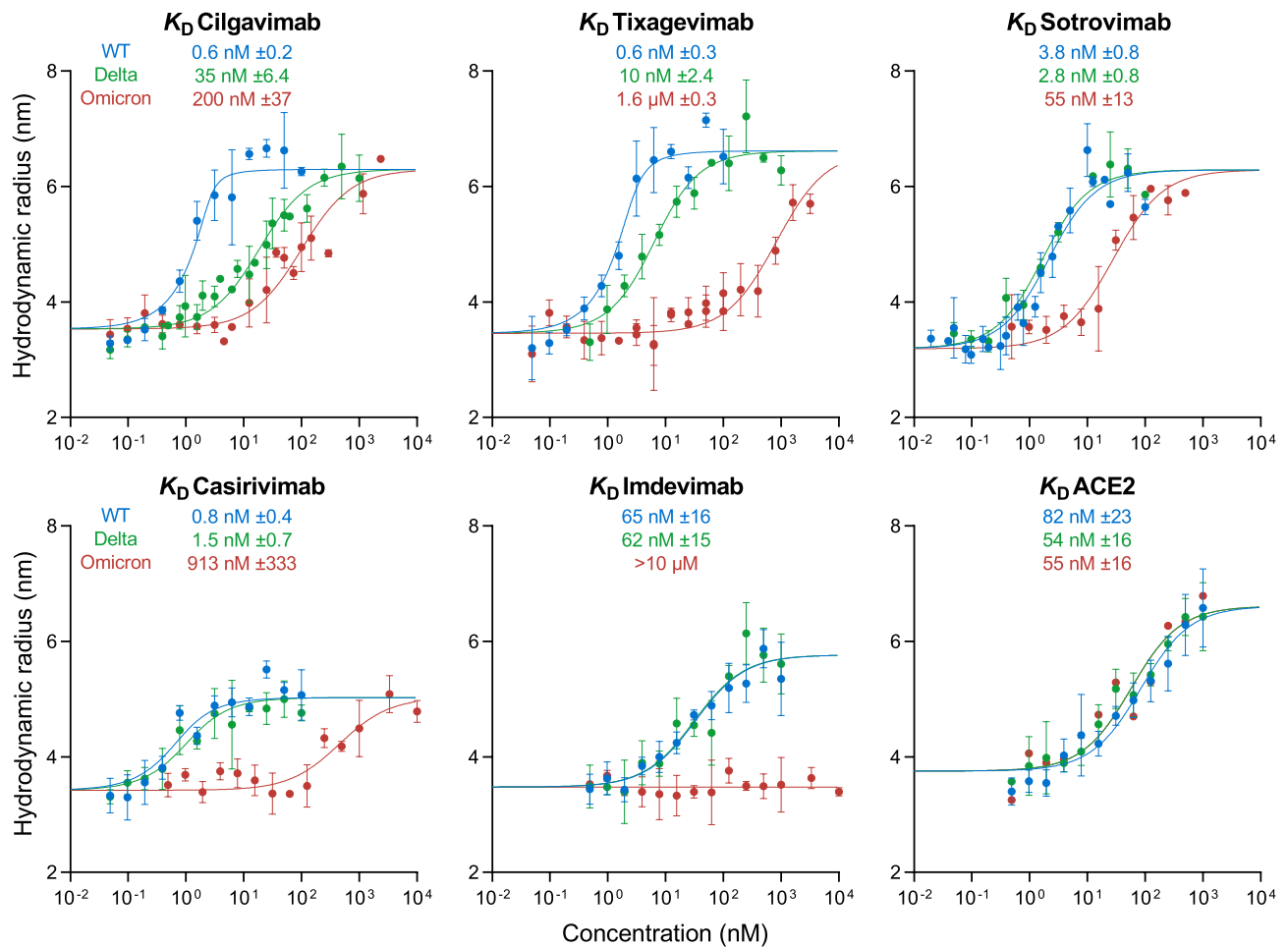


Figure 1. Equilibrium binding curves of cilgavimab, tixagevimab, sotrovimab, casirivimab, imdevimab, and ACE2 binding to spike RBD proteins from SARS-CoV-2 wild type (blue) as well as variants Delta (green) and Omicron BA.1 (red) as determined by microfluidic diffusional sizing (MDS). Error bars are standard deviations from triplicate measurements. K_D values are best fits with standard errors from non-linear least squares fits in terms of a 2:1 binding model (antibodies) or a 1:1 binding model (ACE2).

E484A, Q493R are all within 5 Å of the antibody, while imdevimab is within 5 Å of the mutations N440K and Q498R (Fig. 2).

Relative to wild type RBD, only cilgavimab and tixagevimab showed a reduced binding affinity to Delta RBD (Fig. 3A). For Omicron BA.1 RBD, cilgavimab, tixagevimab, casirivimab, and imdevimab displayed binding affinities reduced by at least two orders of magnitude. Due to its highly conserved epitope³⁰, the affinity of sotrovimab to Omicron BA.1 RBD was reduced by only a factor of 10.

The affinities of both Delta and Omicron BA.1 RBD for ACE2 are very similar to that of wild type RBD (Fig. 3A). In the case of Delta RBD, this would be expected as this variant does not carry any changes in the ACE2 binding interface⁴. Omicron BA.1 RBD, on the other hand, has eight substitutions in the ACE2 binding interface⁴, so it is surprising that the binding affinity is not impacted. These data highlight the critical role this interaction plays in viral replication and hence the selective pressure on RBD mutants to maintain efficient ACE2 binding. Given the retained ACE2 affinity of the Omicron BA.1 variant, cilgavimab, tixagevimab, and casirivimab, which inhibit viral ACE2 binding, would require extremely high concentrations to achieve relevant levels of inhibition due to their strongly reduced affinity.

The changes in affinities, relative to the wild type RBD, of these five antibodies that result from the Delta and Omicron BA.1 mutations suggest close correlations between in-solution binding affinity measurements and changes in antiviral activity. As shown in Fig. 3B, our in-solution affinity measurements are excellent surrogates (Pearson correlation coefficient $R = 0.8$, p -value = 1.4×10^{-7}) for EC_{50} and IC_{50} values obtained by focus reduction neutralization tests and pseudovirus neutralization assays^{3,5-9}. For example, each of casirivimab, imdevimab, and sotrovimab have similar changes in affinities and in EC_{50}/IC_{50} values when challenged with wild type or Delta RBDs. When challenged with the Omicron BA.1 variant, all tested antibodies except sotrovimab experience strong reduction in affinity in line with strong decrease in IC_{50} values. Sotrovimab retains both considerable binding affinity and neutralization efficacy. The strong correlation of in-solution K_D and EC_{50}/IC_{50} values raises the prospect of a straight-forward method informing on antiviral activity. MDS provides universally comparable

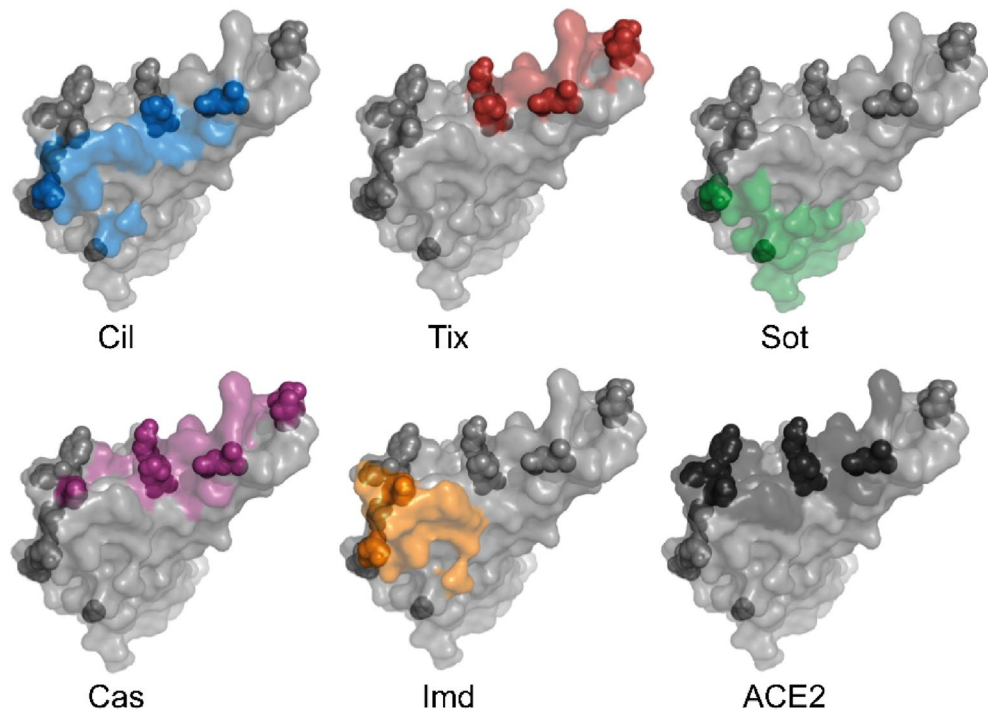


Figure 2. Omicron BA.1 spike mutations compared to antibody epitopes and the ACE2 binding motif. RBD is shown as grey surface with residues within 5 Å of indicated interacting partner colored and Omicron BA.1 mutations shown as spheres. PDB codes for structures are: 7L7E²⁵ (cilgavimab and tixagevimab), 7SOC²⁶ (sotrovimab), 6XDG²³ (casirivimab and imdevimab), and 7DQA²⁷ (ACE2).

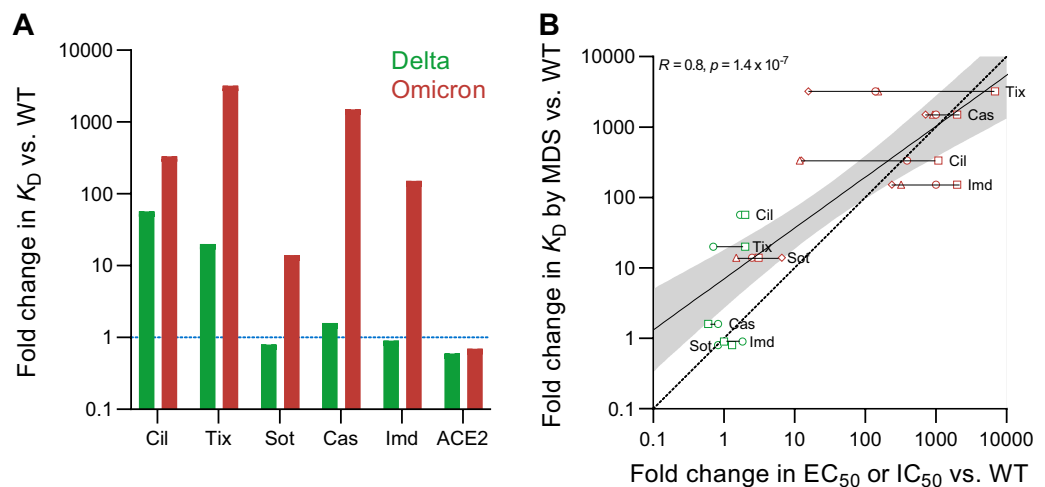


Figure 3. (A) Affinity (K_D) changes of therapeutic COVID-19 antibodies and ACE2 in the presence of Delta (green) and Omicron BA.1 (red) spike RBDs as compared with wild type RBD. (B) K_D changes of therapeutic COVID-19 antibodies correlated with their published half-maximal effective concentrations (EC_{50}) or half-maximal inhibitory concentrations (IC_{50}) of focus reduction neutralization tests (FRNT; active virus) or pseudovirus neutralization tests (PNT), respectively. Triangles and diamonds are FRNTs using VERO-TMPRSS2 and VERO-hACE2-TMPRSS2 cells, respectively, taken from VanBlargan et al.⁷. Squares and circles are PNTs taken from Cao et al.⁵ and Liu et al.⁶, respectively. The solid line is a linear regression with the gray area indicating the 95% confidence intervals, R the Pearson's correlation coefficient and the p -value demonstrating statistical significance. The dashed line indicates the ideal scenario of change in K_D being equal to change in EC_{50} or IC_{50} .

results in the form of absolute affinities (K_D), requires less than 1 h, uses less than 4 μg of antibody, and is simple to perform as no cell culture or handling of active viruses is required. In addition to being much more time consuming and complex experiments, virus neutralization assays can yield variable results depending, for example, on the exact type of assay that is used (Fig. 3B). Here, MDS can serve as a complementary method to support observations made in more complex biological systems that, for example, take the effector function of antibody isotypes²² and its influence on the immune responses into account.

Next, we analyzed how the spike RBD binding affinities of cilgavimab, tixagevimab, sotrovimab, casirivimab, and imdevimab compared to polyclonal antibody responses in unvaccinated COVID-19 convalescent individuals (Fig. 4). Generally, affinities of serum antibodies and their specific concentrations are difficult to measure. To address this issue, we recently introduced microfluidic antibody affinity profiling (MAAP)^{18–21} as an advanced serological assay which utilizes equilibrium, in-solution binding measurements based on size change of a fluorescently labeled antigen to measure antibody affinities and concentrations directly in serum or plasma. This quantitative view on the functional immune response of individuals is advantageous over commonly measured antibody titers, which are a combination of both affinity and concentration. MAAP was used in several previous studies^{18,20,21} (see Table S3 for details) to determine the affinity and concentration of wild type RBD-specific antibodies. For this paper, we collated these previously published results to provide the overall affinity range and concentration range of antibodies found in convalescent, unvaccinated individuals (Fig. 4A). Both affinity and concentration of wild type specific RBD antibodies vary over several orders of magnitude between individuals. However, 75% of samples contained antibodies with affinities greater than 10^8 nM^{-1} ($K_D \leq 10 \text{ nM}$) and total binding site concentrations $\leq 150 \text{ nM}$ (Fig. 4A).

Next, we assessed how the antibody affinity and the binding site concentration in a pooled standard plasma from several convalescent donors responds to Omicron BA.1 spike RBD (Fig. 4A). For this experiment, we performed MAAP on the working reagent for anti-SARS-CoV-2 immunoglobulin, which is pooled plasma from COVID-19 convalescent individuals collected between April and May 2020²⁴. Antibody affinities and concentrations against wild type RBD were well within the range observed for most of the individual samples (Fig. 4). When challenged with Delta spike RBD, the affinity of antibodies in the pooled plasma decreased slightly by a factor of approximately 1.5 while the concentration of binding sites remained largely unchanged. Surprisingly, the antibody affinity and concentration against Omicron BA.1 spike RBD were reduced by factors of just 2.5 and 2.0, respectively, compared to wild type. The binding site concentration is still fourfold higher than K_D (ie antibody concentration twofold higher than K_D) suggesting that these polyclonal antibody mixtures retain binding capability against Omicron BA.1 spike RBD. This observation is in line with reports that a considerable population retain some degree of Omicron BA.1 neutralization after infection with wild type or Alpha strains⁹. During infection, highly neutralizing antibodies with high affinity arise very quickly, such that just 2 mutations from germline can boost affinity 100-fold. However, the vast majority of induced antibodies against SARS-CoV-2 remain near-germline and thus can be more promiscuous for epitope mutations^{35–37}.

Next, we were interested to assess the behavior of the monoclonal therapeutic antibodies in the context of the humoral response that results from infection. Cilgavimab, tixagevimab, casirivimab, and imdevimab are derived from convalescent individuals that had been exposed to wild type RBD early in the pandemic²³. Sotrovimab was obtained from a patient who was exposed to the SARS virus during the early 2000s³⁸. As might be expected, the affinities for wild type RBD of the monoclonal antibodies that compete directly with ACE2 binding (Fig. 4C: casirivimab; Fig. 4E,F: tixagevimab and cilgavimab) are tighter than the majority of the population's polyclonal antibody response to the same antigen. Sotrovimab (Fig. 4A) and imdevimab (Fig. 4D) are located in the same region of the plots indicative of slightly lower affinities than the typical polyclonal response.

The reduction in affinity of tixagevimab and cilgavimab against Delta brings them within the range of the polyclonal anti-wild type RBD antibody response produced by most convalescent individuals. On the other hand, casirivimab, imdevimab and sotrovimab do not show a considerable shift when challenged with Delta RBD, with their affinity being largely unaffected. Against Omicron BA.1, all antibodies, except sotrovimab, are either within or close to the regime for which less than 50% of target can be bound (grey area) and so would be expected to provide minimal therapeutic benefit.

Polyclonal anti-wild type RBD antibodies constitute a mixture of non-NABs and NABs, with NABs varying in their neutralization mechanisms^{5,35–37}. Regardless of their mechanisms, loss of NAB binding affinity correlates with viral immune escape^{35–37} (Fig. 3B), as RBD binding is a pre-requisite for neutralization. In addition to the NAB affinity, the degree to which NABs bind is determined by the viral load (i.e., the antigen concentration) and the NAB concentration. With reduced affinity, higher NAB concentrations are required to achieve the same levels of binding for a given viral load. If the affinity is too low, even very high NAB concentrations are not sufficient to achieve considerable binding. Since 60% of anti-RBD antibodies isolated from convalescent individuals showed neutralization³⁷, a reduction in the average affinity of a polyclonal NAB mixture is likely linked to reduced virus neutralization.

Figure 4 shows that compared with the therapeutic monoclonal antibodies, most individual sera and plasmas have rather low affinity and only very few demonstrate picomolar affinities. For such moderate affinity antibodies, a drop in affinity due to epitope changes is likely to be less profound than for antibodies with high affinity. For the latter, epitope mutation can be detrimental as evidenced by the profoundly reduced affinities of casirivimab, tixagevimab, and cilgavimab, for example.

Another aspect of study is that the samples from unvaccinated, convalescent individuals were taken in 2020, so while exact virus variants have not been confirmed for these cohorts it is highly likely these individuals will have developed an immune response against an early version of SARS-CoV-2 (for example Wuhan-Hu-1). Since most vaccines are based on early variants of SARS-CoV-2, it is of great interest to compare serological fingerprints to RBD of wild type, delta, and omicron BA.1 variants of the here analyzed convalescent cohorts exposed to an early SARS-CoV-2 variant to those of vaccinated individuals. In a study run in parallel to the one presented

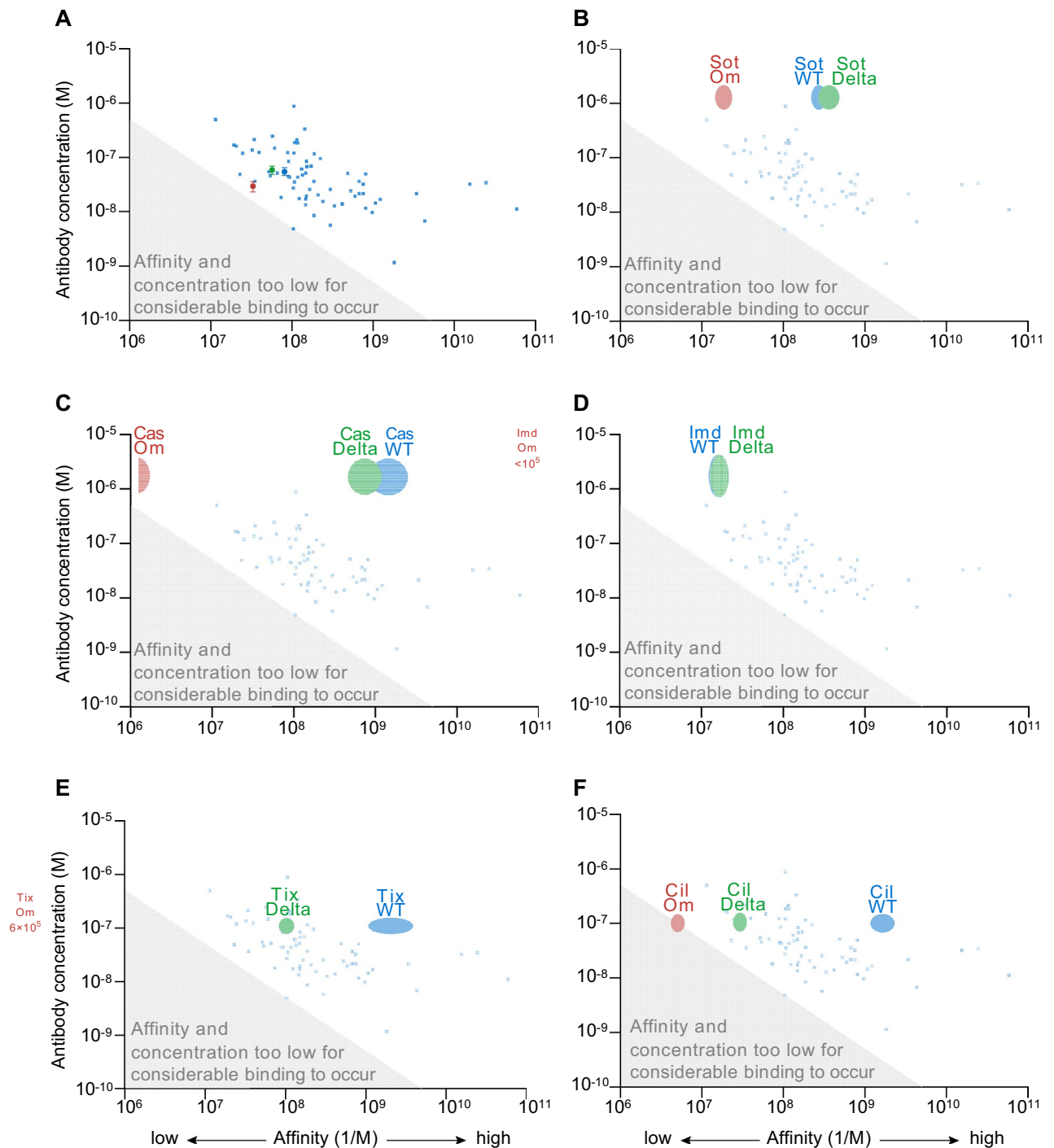


Figure 4. Affinities and average maximum post-dosage concentrations of therapeutic antibodies in comparison with affinities and concentrations of serum or plasma of COVID-19 convalescent individuals. (A) serological fingerprints of COVID-19 unvaccinated, convalescent individuals (see Table S3 for details) using wild type RBD as an antigen in context with fingerprints of the working reagent for anti-SARS-CoV-2 immunoglobulin²⁴ (pooled plasma of COVID-19 convalescents) using wild type spike RBD (blue), Delta spike RBD (green), or Omicron BA.1 spike RBD (red) as antigens. The shaded gray region of the plot indicates the area where antibody concentration is less than $K_D/2$ such that binding site concentration is less than K_D and so binding is not able to exceed 50%. (B–F) Affinities of (B) sotrovimab, (C) casirivimab, (D) imdevimab, (E) tixagevimab, and (F) cilgavimab in comparison with the serological fingerprints of convalescent donors shown in (A). The width and height of the monoclonal antibody ovals are the standard error affinities (K_A determined by MDS) against wild type spike RBD (blue), Delta spike RBD (green), or Omicron BA.1 spike RBD (red) and maximum serum concentrations obtained after dosage^{32–34} (average \pm 1 SD), respectively.

here²², we found that indeed vaccinated individuals showed similar serological fingerprints as compared with convalescents or with individuals at various stages of infection. Future studies need to address how affinity and concentration of RBD-specific antibodies change over time and how this correlates with vaccine efficacy, disease severity, and the medical history of individuals.

Conclusions

Using microfluidic diffusional sizing, we quantified the binding affinities of five therapeutic antibodies to spike receptor binding domains of the wild type variant, the Delta variant, and the Omicron BA.1 variant of SARS-CoV-2. The affinities of cilgavimab, tixagevimab, casirivimab, and imdevimab to Omicron BA.1 spike RBD were reduced by several orders of magnitude, whereas sotrovimab retained considerable binding affinity. These affinity reductions in the presence of Omicron BA.1 RBD agree very well with the reduced antiviral activity of these antibodies for which sotrovimab is also the least affected. These results suggest that simple in-solution affinity measurements can serve to evaluate antiviral activity before complex and time-consuming virus neutralization assays are performed. Serological fingerprints generated by microfluidic antibody affinity profiling of samples from COVID-19 convalescent individuals reveal serum-antibody affinity and concentration and provide further context to this finding. Out of the five tested antibodies, only sotrovimab retained affinities similar to those of polyclonal antibodies specific for wild type RBD, which is again indicative of its high antiviral activity against the Omicron BA.1 variant. Our results represent a new way of linking monoclonal antibody affinities with their antiviral activity and serological fingerprints, which has the potential to guide the development of new therapeutics to fit the affinity window of antibodies generated by the humoral immune response.

Materials and methods

Sample collection, ethics, and biosafety. All plasma and serum samples were collected from unvaccinated convalescent individuals. Unless otherwise stated, no information regarding the application of therapeutic antibodies, immunosuppressant drugs or other therapeutic agents was available for the purposes of this study. All such sample collection was performed in accordance with the provisions of the Declaration of Helsinki and the Good Clinical Practice guidelines of the International Conference on Harmonization as detailed below:

For all samples^{20,39,40} collected by University Hospital Zurich. All experiments and analyses involving samples from human donors were conducted with the approval of the local ethics committee, Kantonale Ethik-Kommission des Kantons Zürich (KEK-ZH-Nr.2015-0561, BASEC-Nr. 2018-01042, and BASEC-Nr. 2020-01731), in accordance with the provisions of the Declaration of Helsinki and the Good Clinical Practice guidelines of the International Conference on Harmonization.

EDTA plasma from healthy donors and from convalescent individuals was obtained from the Blutspendedienst (BDS) Kanton Zürich from donors who signed the consent that their samples can be used for conducting research. Samples from patients with COVID-19 were collected at the University Hospital Zurich from patients who signed an informed consent.

For all samples collected by the Fred Hutchinson Cancer Research Center and the University of Washington. Sample collection and following experiments and analyses were conducted in accordance with Fred Hutch and University of Washington Institutional Review Board (IRB) approved protocols. Informed consent was obtained from all human subjects. Plasma samples from SARS-CoV-2 seropositive individuals were obtained from a Fred Hutch repository and from the repository of the University of Washington. FHCRC repository was assembled from a COVID-19 seroepidemiology study conducted in a single county in the western US (FHCRC IRB #10453)⁴¹. UW repository was formed from Seattle-area participants recruited for potential donation of single-donor plasma units (ClinicalTrials.gov: NCT04338360), and plasma for manufacture of a pooled anti-SARS-CoV-2 product (NCT04344977)⁴².

For all samples collected by Mayo Clinic. Samples were residual waste specimens that were fully deidentified and handled according to the policies (including those governing informed consent) of the Mayo Clinic Institutional Review Board (IRB). The IRB review processes are based on the Federal Policy for the Protection of Human Subjects ("Common Rule"), the Belmont Report and provisions of 45CFR46—"Protection of Human Subjects". These policies deem it unnecessary to secure informed consent for the use of de-identified clinical waste specimens.

Fluorescent labeling of proteins. Recombinant proteins (please see Tables 1 and 2 for details) were labeled with Alexa Fluor™ 647 NHS ester (Thermo Fisher) as described previously¹⁸. In brief, solution containing 150 µg of spike RBD was mixed with dye at a three-fold molar excess in the presence of NaHCO₃ (Merck) buffer at pH 8.3 and incubated at 4 °C overnight. Unbound label was removed by size-exclusion chromatography (SEC) on an ÄKTA pure system (Cytiva) using a Superdex 75 Increase 10/300 column (Cytiva). Labeled and purified proteins were stored at –80 °C in PBS pH 7.4 containing 10% (w/v) glycerol as cryoprotectant.

Equilibrium binding measurements by microfluidic diffusional sizing (MDS). Binding affinity of antibodies and spike RBD proteins was measured on a Fluidity One-M (Fluidic Analytics). Fluorescently labeled RBD at a concentration of 1 nM or 5 nM was mixed with unlabelled antibody at 12 different, decreasing concentrations of a two-fold dilution series and incubated on ice for at least 30 min. PBS-Tween 20 (0.05%) pH 7.5 was used as a dilution buffer. Before the measurement, 3.5 µL of PBS-Tween 20 (0.05%) pH 7.5 was transferred

Protein name	SARS-CoV-2 variant	Pango lineage	Vendor	Article number	Amino-acid sequence	Tags	Mutated amino-acid residues
Wild type spike RBD (UniProt P0DTC2)	Wuhan-Hu-1 sequence (NC_045512)	A	Sino Biological	40592-V08H	R319-F541	C-His	
Delta spike RBD (UniProt P0DTC2)	Delta	B.1.617.2	Sino Biological	40592-V08H90	R319-F541	C-His	L452R, T478K
Omicron BA.1 spike RBD (UniProt P0DTC2)	Omicron BA.1	B.1.1.529.1	Sino Biological	40592-V08H121	R319-F541	C-His	G339D, S371L, S373P, S375F, K417N, N440K, G446S, S477N, T478K, E484A, Q493R, G496S, Q498R, N501Y, Y505H

Table 1. Summary of SARS-CoV-2 spike RBD reagents used in this study.

Antibody name	Alternative name	Drugbank code	Vendor	Article number
Tixagevimab Biosimilar	AZD8895	DB16394	ProteoGenix	PX-TA1032
Cilgavimab Biosimilar	AZD1061	DB16393	ProteoGenix	PX-TA1033
Sotrovimab Biosimilar	VIR-7831	DB16355	ProteoGenix	PX-TA1637
Casirivimab	REGN10933	DB15941	ProteoGenix	PTXCOV-A552
Imdevimab	REGN10987	DB15940	ProteoGenix	PTXCOV-A553

Table 2. Summary of antibody reagents used in this study.

to each of the 24 flow buffer ports of the Fluidity-One M chip plate, and the microfluidic circuits were allowed to prime for at least 1 min. Then, 2 times 3.5 μ L of the 12 different RBD–antibody mixtures were transferred to the 24 sample ports of the Fluidity One-M chip plate to measure a binding curve of 12 antibody concentrations in duplicate. On the Fluidity One-M, the Alexa-647 detection setting and size-range setting of 3–14 nm was used. K_D values were determined by non-linear least squares fitting as described previously¹⁸ using Prism (GraphPad Software). Linear regression to analyze the correlation between antibody K_D values and antiviral activity was calculated in ggplot2⁴³ and regression coefficients were computed using the `stat_cor()` function as part of the ggpubr (version 0.4.0) package. We display the Pearson correlation coefficient R .

Microfluidic antibody affinity profiling (MAAP) on the working reagent for anti-SARS-CoV-2 immunoglobulin. The working reagent for anti-SARS-CoV-2 immunoglobulin (National Institute for Biological Standards and Control 21/234) is a calibrated product equivalent to the high concentration sample (NIBSC 20/150) from the WHO working standard for anti-SARS-CoV-2 immunoglobulin (NIBSC 20/268). NIBSC 21/234 consist of pooled plasma from individuals who recovered from COVID-19 and was collected between April and May 2020²⁴. MAAP was performed as described previously^{18–22}. In brief, fluorescently labelled spike RBD from wild type, Delta, and Omicron BA.1 was mixed with various dilutions of plasma from convalescent donors and incubated on ice for at least 30 min. A buffer containing PBS at pH 7.4, 10% glycerol, and 5% (w/v) human serum albumin was used for plasma dilutions. Equilibrium binding of RBD to plasma antibodies was assessed by monitoring hydrodynamic radii (R_h) on the Fluidity One-M. The measurement protocol was the same as for purified proteins measured in buffer, with the only difference being that 3.5 μ L of the plasma sample instead of PBS-Tween (0.05%) was added to the flow buffer ports of the Fluidity One-M chip plate. Bayesian inference was used to determine K_D and binding site concentrations from the mode of the joint posterior distribution, also as described previously^{18–22}.

Data availability

Sequences of proteins used in this study have been deposited in publicly available databases. Please refer to Tables 1 and 2 for details.

Received: 21 March 2022; Accepted: 11 October 2022

Published online: 17 November 2022

References

1. WHO. Classification of Omicron (B.1.1.529): SARS-CoV-2 Variant of Concern (accessed 27 December 2021); [https://www.who.int/news/item/26-11-2021-classification-of-omicron-\(b.1.1.529\)-sars-cov-2-variant-of-concern](https://www.who.int/news/item/26-11-2021-classification-of-omicron-(b.1.1.529)-sars-cov-2-variant-of-concern)
2. Karim, S. S. A. & Karim, Q. A. Omicron SARS-CoV-2 variant: A New chapter in the COVID-19 pandemic. *Lancet* **398**(10317), 2126–2128. [https://doi.org/10.1016/S0140-6736\(21\)02758-6/ATTACHMENT/B8C47DC8-B485-4240-95DD-FF7ADBB31E18/MMC1.PDF](https://doi.org/10.1016/S0140-6736(21)02758-6/ATTACHMENT/B8C47DC8-B485-4240-95DD-FF7ADBB31E18/MMC1.PDF) (2021).
3. Camerini, E. *et al.* Broadly neutralizing antibodies overcome SARS-CoV-2 omicron antigenic shift. *Nature* **602**, 664–670. <https://doi.org/10.1038/D41586-021-03825-4> (2021).
4. Han, P. *et al.* Receptor binding and complex structures of human ACE2 to spike RBD from omicron and delta SARS-CoV-2. *Cell* **185**(4), 630–640. <https://doi.org/10.1016/J.CELL.2022.01.001> (2022).

5. Cao, Y. *et al.* Omicron escapes the majority of existing SARS-CoV-2 neutralizing antibodies. *Nature* **602**, 657–663. <https://doi.org/10.1038/D41586-021-03796-6> (2021).
6. Liu, L. *et al.* Striking antibody evasion manifested by the omicron variant of SARS-CoV-2. *Nature* **602**, 676–681. <https://doi.org/10.1038/D41586-021-03826-3> (2021).
7. VanBlargan, L. A. *et al.* An infectious SARS-CoV-2 B.1.1.529 omicron virus escapes neutralization by therapeutic monoclonal antibodies. *Nat. Med.* **28**(3), 490–495. <https://doi.org/10.1038/s41591-021-01678-y> (2022).
8. Dejnirattisai, W. *et al.* SARS-CoV-2 omicron-B.1.1.529 leads to widespread escape from neutralizing antibody responses. *Cell* **185**(3), 467–484. <https://doi.org/10.1016/j.cell.2021.12.046> (2022).
9. Planas, D. *et al.* Considerable escape of SARS-CoV-2 omicron to antibody neutralization. *Nature* **602**, 671–675. <https://doi.org/10.1038/D41586-021-03827-2> (2021).
10. Dejnirattisai, W. *et al.* Reduced neutralisation of SARS-CoV-2 omicron B.1.1.529 variant by post-immunisation serum. *Lancet* **399**(10321), 234–236. [https://doi.org/10.1016/S0140-6736\(21\)02844-0](https://doi.org/10.1016/S0140-6736(21)02844-0) (2021).
11. Lu, L. *et al.* Neutralization of severe acute respiratory syndrome coronavirus 2 omicron variant by sera from BNT162b2 or CoronaVac vaccine recipients. *Clin. Infect. Dis.* **75**(1), e822–e826. <https://doi.org/10.1093/cid/ciab1041> (2022).
12. Bentley, E. G., Kirby, A., Sharma, P., Kipar, A., Mega, D. F., Bramwell, C., Penrice-Randal, R., Prince, T., Brown, J. C., Zhou, J., Screaton, G. R., Barclay, W. S., Owen, A., Hiscox, J. A. & Stewart, J. P. SARS-CoV-2 Omicron-B.1.1.529 variant leads to less severe disease than pango b and delta variants strains in a mouse model of severe COVID-19. *bioRxiv* **2021**, 2021.12.26.474085. <https://doi.org/10.1101/2021.12.26.474085>
13. Abdelnabi, R. *et al.* The Omicron (B.1.1.529) SARS-CoV-2 variant of concern does not readily infect syrian hamsters. *Antiviral Res.* **198**, 105253. <https://doi.org/10.1016/j.antiviral.2022.105253> (2022).
14. Halfmann, P. J. *et al.* SARS-CoV-2 omicron virus causes attenuated disease in mice and hamsters. *Nature* **603**(7902), 687–692. <https://doi.org/10.1038/s41586-022-04441-6> (2022).
15. Wolter, N. *et al.* Early assessment of the clinical severity of the SARS-CoV-2 omicron variant in South Africa: A data linkage study. *Lancet* **399**(10323), 437–446. [https://doi.org/10.1016/S0140-6736\(22\)00017-4](https://doi.org/10.1016/S0140-6736(22)00017-4) (2022).
16. Meng, B. *et al.* Altered TMPRSS2 usage by SARS-CoV-2 omicron impacts infectivity and fusogenicity. *Nature* **603**(7902), 706. <https://doi.org/10.1038/S41586-022-04474-X> (2022).
17. Hui, K. P. Y. *et al.* SARS-CoV-2 omicron variant replication in human bronchus and lung ex vivo. *Nature* **603**(7902), 715–720. <https://doi.org/10.1038/s41586-022-04479-6> (2022).
18. Fiedler, S. *et al.* Antibody affinity governs the inhibition of SARS-CoV-2 Spike/ACE2 binding in patient serum. *ACS Infect. Dis.* **7**(8), 2362–2369. <https://doi.org/10.1021/acsinfecdis.1c00047> (2021).
19. Schneider, M. M., Scheidt, T., Priddey, A. J., Xu, C. K., Hu, M., Devenish, S. R. A., Meisl, G., Dobson, C. M., Kosmoliaptis, V. & Knowles, T. P. J. Microfluidic Antibody Affinity Profiling for In-Solution Characterisation of Alloantibody - HLA Interactions in Human Serum. *bioRxiv*. bioRxiv September 2020, p 2020.09.14.296442. <https://doi.org/10.1101/2020.09.14.296442>
20. Schneider, M. M. *et al.* Microfluidic characterisation reveals broad range of SARS-CoV-2 antibody affinity in human plasma. *Life Sci. Alliance* **5**(2), e202101270. <https://doi.org/10.26508/LSA.202101270> (2022).
21. Denninger, V. *et al.* Microfluidic antibody affinity profiling reveals the role of memory reactivation and cross-reactivity in the defense against SARS-CoV-2. *ACS Infect. Dis.* **8**(4), 790–799. https://doi.org/10.1021/ACSINFECDIS.IC00486/ASSET/IMAGES/MEDIUM/ID1C00486_M005.GIF (2022).
22. Emmenegger, M. *et al.* Both COVID-19 infection and vaccination induce high-affinity cross-clade responses to SARS-CoV-2 variants. *iScience* **25**(8), 2022.04.07.22273545. <https://doi.org/10.1016/J.ISCI.2022.104766> (2022).
23. Hansen, J. *et al.* Studies in humanized mice and convalescent humans yield a SARS-CoV-2 antibody cocktail. *Science* **369**(6506), 1010–1014. https://doi.org/10.1126/SCIENCE.ABD0827/SUPPL_FILE/ABD0827_MDAR-REPRODUCIBILITYCHECKLIST.PDF (2020).
24. Mattiuzzo, G., Bentley, E. M., Hassall, M., Routley, S., Richardson, S., Bernasconi, V., Kristiansen, P., Harvala, H., Roberts, D., Semple, M. G., Cw Turtle, L., Openshaw, P. J., Baillie, K., Sofie, L., Nissen-Meyer, H., Broch Brantsaeter, A., Baxendale, H., Atkinson, E., Rigby, P., Padley, D., Almond, N., Rose, N. J. & Page, M. Establishment of the WHO International Standard and Reference Panel for Anti-SARS-CoV-2 Antibody on Behalf of the ISARIC4C Investigators. *WHO* **2020**.
25. Dong, J. & Crowe, J. E. Crystal structure of SARS-CoV-2 spike RBD in complex with human monoclonal antibodies AZD8895 and AZD1061. *PDB* <https://doi.org/10.2210/pdb717e/pdb> (2021).
26. McCallum, M. *et al.* Molecular basis of immune evasion by the delta and kappa SARS-CoV-2 variants. *Science* **374**(6575), 1621–1626. <https://doi.org/10.1126/SCIENCE.ABL8506> (2021).
27. Wang, J., Lan, J., Wang, X. Q. & Wang, H. W. Cryo-EM structure of SARS-CoV2 RBD-ACE2 complex. *PDB* <https://doi.org/10.2210/pdb7dqa/pdb> (2021).
28. Dong, J. *et al.* Genetic and structural basis for SARS-CoV-2 variant neutralization by a two-antibody cocktail. *Nat. Microbiol.* **6**(10), 1233–1244. <https://doi.org/10.1038/s41564-021-00972-2> (2021).
29. Zost, S. J. *et al.* Potently neutralizing and protective human antibodies against SARS-CoV-2. *Nature* **584**, 443–449. <https://doi.org/10.1038/s41586-020-2548-6> (2020).
30. Cathcart, A. L. *et al.* The dual function monoclonal antibodies VIR-7831 and VIR-7832 demonstrate potent in vitro and in vivo activity against SARS-CoV-2. *bioRxiv* <https://doi.org/10.1101/2021.03.09.434607> (2021).
31. Tuccori, M. *et al.* Anti-SARS-CoV-2 neutralizing monoclonal antibodies: Clinical pipeline. *MAbs* **12**(1), e1854149. <https://doi.org/10.1080/19420862.2020.1854149> (2020).
32. Weinreich, D. M. *et al.* REGN-COV2, a neutralizing antibody cocktail, in outpatients with covid-19. *N. Engl. J. Med.* **384**(3), 238–251. https://doi.org/10.1056/NEJMOA2035002/SUPPL_FILE/NEJMOA2035002_DATA-SHARING.PDF (2021).
33. CHMP. Art 5(3) - Sotrovimab (VIR-7831 - GSK4182136) for the Treatment of COVID-19 (GSK) - Assessment Report. **2021**.
34. FACT SHEET FOR HEALTHCARE PROVIDERS: EMERGENCY USE AUTHORIZATION FOR EVUSHELD™ (Tixagevimab Co-Packaged with Cilgavimab) HIGHLIGHTS OF EMERGENCY USE AUTHORIZATION (EUA) These Highlights of the EUA Do Not Include All the Information Needed to Use EVUSHELD™ under the EUA. See the FULL FACT SHEET FOR HEALTHCARE PROVIDERS for EVUSHELD. **2020**.
35. Barnes, C. O. *et al.* SARS-CoV-2 neutralizing antibody structures inform therapeutic strategies. *Nature* **588**, 682–687. <https://doi.org/10.1038/s41586-020-2852-1> (2020).
36. Yuan, M. *et al.* Structural and functional ramifications of antigenic drift in recent SARS-CoV-2 variants. *Science* **373**(6556), 818–823. <https://doi.org/10.1126/SCIENCE.ABH1139> (2021).
37. Dejnirattisai, W. *et al.* The antigenic anatomy of SARS-CoV-2 receptor binding domain. *Cell* **184**(8), 2183–2200.e22. <https://doi.org/10.1016/J.CELL.2021.02.032> (2021).
38. Pinto, D. *et al.* Cross-neutralization of SARS-CoV-2 by a human monoclonal SARS-CoV antibody. *Nature* **583**(7815), 290–295. <https://doi.org/10.1038/s41586-020-2349-y> (2020).
39. Emmenegger, M. *et al.* Continuous population-level monitoring of SARS-CoV-2 seroprevalence in a large metropolitan region. *Medrxiv* <https://doi.org/10.1101/2020.05.31.20118554> (2022).
40. Emmenegger, M. I. *et al.* Anti-prothrombin autoantibodies enriched after infection with SARS-CoV-2 and influenced by strength of antibody response against SARS-CoV-2 proteins. *PLOS Pathog.* **17**(12), e1010118. <https://doi.org/10.1371/JOURNAL.PPAT.1010118> (2021).

41. McLaughlin, C. C. *et al.* High community SARS-CoV-2 antibody seroprevalence in a ski resort community, Blaine County, Idaho, U.S. preliminary results. *Medrxiv Prepr. Serv. Heal. Sci.* <https://doi.org/10.1101/2020.07.19.20157198> (2020).
42. Boonyaratanakornkit, J. *et al.* Clinical, laboratory, and temporal predictors of neutralizing antibodies against SARS-CoV-2 among COVID-19 convalescent plasma donor candidates. *J. Clin. Invest.* **131**(3), e144930. <https://doi.org/10.1172/JCI144930> (2021).
43. Wickham, H. *Ggplot2: Elegant Graphics for Data Analysis* (Springer, 2016).

Author contributions

S.F.: conceptualization, data curation, formal analysis, supervision, investigation, visualization, methodology, project administration and writing—original draft, review and editing. S.R.A.D.: conceptualization, data curation, formal analysis, supervision, investigation, visualization, methodology, project administration and writing—original draft, review and editing. A.S.M.: conceptualization, data curation, formal analysis, supervision, investigation, visualization, methodology, project administration and writing—original draft, review and editing. A.I.: data curation and writing—review and editing. F.R.: data curation and writing—review and editing. M.E.: data curation and writing—review and editing. V.K.: conceptualization, writing—review. E.S.T.: conceptualization, resources, data curation, funding acquisition and writing—review. J.R.M.: conceptualization, resources, data curation, funding acquisition and writing—review. A.M.S.: conceptualization, data curation, investigation, visualization, project administration and writing—original draft, review and editing. A.A.: conceptualization, resources, supervision, and writing—original draft, review, and editing. A.I.: conceptualization, supervision, and writing—original draft, review, and editing. A.K.L.: conceptualization, resources, data curation, visualization, project administration, funding acquisition and writing—review and editing. T.P.J.K.: conceptualization, resources, supervision, funding acquisition, methodology, and writing—original draft, review, and editing.

Funding

Institutional core funding by the University of Zurich and the University Hospital of Zurich, as well as Driver Grant 2017DRI17 of the Swiss Personalized Health Network to A.A.; funding by Grants of Innovation Fund of the University Hospital Zurich (INOV00096), and of the NOMIS Foundation, the Schwyzer Winiker Stiftung, and the Baugarten Stiftung (coordinated by the USZ Foundation, USZF27101) to A.A. and M.E. V.K. was funded by an NIHR fellowship (PD-2016-09-065). T.P.J.K. is grateful for financial support by the Biotechnology and Biological Sciences Research Council and the European Research Council.

Competing interests

T.P.J.K. is a member of the board of directors of Fluidic Analytics. AA is a member of the clinical and scientific advisory board of Fluidic Analytics. V.K. is a consultant for Fluidic Analytics. S.F., S.R.A.D., A.S.M., A.I., F.R., and A.K.L. are employees of Fluidic Analytics.

Additional information

Supplementary Information The online version contains supplementary material available at <https://doi.org/10.1038/s41598-022-22214-z>.

Correspondence and requests for materials should be addressed to S.F. or T.P.J.K.

Reprints and permissions information is available at www.nature.com/reprints.

Publisher's note Springer Nature remains neutral with regard to jurisdictional claims in published maps and institutional affiliations.



Open Access This article is licensed under a Creative Commons Attribution 4.0 International License, which permits use, sharing, adaptation, distribution and reproduction in any medium or format, as long as you give appropriate credit to the original author(s) and the source, provide a link to the Creative Commons licence, and indicate if changes were made. The images or other third party material in this article are included in the article's Creative Commons licence, unless indicated otherwise in a credit line to the material. If material is not included in the article's Creative Commons licence and your intended use is not permitted by statutory regulation or exceeds the permitted use, you will need to obtain permission directly from the copyright holder. To view a copy of this licence, visit <http://creativecommons.org/licenses/by/4.0/>.

© The Author(s) 2022